

Robust Gamma Coherence between Macaque V1 and V2 by Dynamic Frequency Matching

Mark J. Roberts,^{1,2,*} Eric Lowet,^{1,2} Nicolas M. Brunet,^{1,4} Marije Ter Wal,¹ Paul Tiesinga,¹ Pascal Fries,^{1,3} and Peter De Weerd^{1,2}

¹Donders Institute for Brain, Behavior and Cognition, Radboud University, 6500 HC Nijmegen, the Netherlands

²Faculty of Psychology and Neuroscience, Maastricht University, 6200 MD Maastricht, the Netherlands

³Ernst Strüngmann Institute (ESI) for Neuroscience in Cooperation with Max Planck Society, 60528 Frankfurt, Germany

⁴Department of Neurological Surgery, University of Pittsburgh, Pittsburgh, PA 15213, USA

*Correspondence: mark.roberts@maastrichtuniversity.nl

<http://dx.doi.org/10.1016/j.neuron.2013.03.003>

SUMMARY

Current theories propose that coherence of oscillatory brain activity in the gamma band (30–80 Hz) constitutes an avenue for communication among remote neural populations. However, reports documenting stimulus dependency and time variability of gamma frequency suggest that distant neuronal populations may, at any one time, operate at different frequencies precluding synchronization. To test this idea, we recorded from macaque V1 and V2 simultaneously while presenting gratings of varying contrast. Although gamma frequency increased with stimulus contrast in V1 and V2 (by ~25 Hz), V1-V2 gamma coherence was maintained for all contrasts. Moreover, while gamma frequency fluctuated by ~15 Hz during constant contrast stimulation, this fluctuation was highly correlated between V1 and V2. The strongest coherence connections showed a layer-specific pattern, matching feedforward anatomical connectivity. Hence, gamma coherence among remote populations can occur despite large stimulus-induced and time-dependent changes in gamma frequency, allowing communication through coherence to operate without a stimulus independent, fixed-frequency gamma channel.

INTRODUCTION

Cortical activity is characterized by oscillatory processes segregated into distinct frequency bands. According to the “communication through coherence” (CTC) hypothesis (Fries, 2005), coherent oscillations in the so-called gamma band (30–80 Hz) contribute importantly to long-range information transmission among different hierarchical processing levels of the brain during sensory and cognitive processing (Fries, 2005; Salinas and Sejnowski, 2001; Tiesinga et al., 2002; Wildie and Shanahan, 2012). Coherence is facilitated when oscillations in distant

areas, or distant regions of the same areas (Gray et al., 1989), occur at the same frequency on a moment-to-moment basis (Buzsáki and Draguhn, 2004; Rosenblum et al., 2001). Until recently, it was thought that gamma frequency was highly stable over time and across brain areas in a given individual (Hoogenboom et al., 2006; Muthukumaraswamy et al., 2010), which would ensure efficient communication among remote neuronal populations.

However, the idea that gamma frequencies in different areas are by default matched across the brain runs counter the fact that gamma depends on local network properties (Buia and Tiesinga, 2006; Fries, 2005), which likely will differ among areas. Therefore, the gamma frequencies exhibiting maximum power (“gamma peak frequencies”) in a given stimulus condition could differ substantially between areas. Moreover, a number of reports have demonstrated strong dependencies of gamma band frequencies on visual stimulus parameters (Feng et al., 2010; Gieselmann and Thiele, 2008; Jia et al., 2013; Ray and Maunsell, 2010, 2011; Swettenham et al., 2009). In view of likely differences among visual areas, variations in low-level stimulus parameters may therefore affect gamma frequency in a way that differs substantially between areas. As a result, gamma frequency differences, coherence, and thus the efficiency of information transfer between remote populations in different visual areas would be stimulus dependent, thereby rendering CTC implausible (Jia et al., 2013). Additionally, gamma power and frequency in V1 have been shown to change rapidly in an apparently random manner during constant stimulation (Burns et al., 2011; Xing et al., 2012a), or in response to fluctuations in the internal state of the animal (Gray and McCormick, 1996). If these rapid variations were to occur in an uncoordinated fashion in different visual areas, a possibility that so far has not been tested, then this would constitute another challenge to CTC. Hence, whenever the frequency in a given area shifts, CTC can only operate efficiently if the gamma frequency in communicating areas is dynamically matched.

Here, we aimed to address the fundamental question of whether gamma frequency modulations induced by stimulus variations or occurring spontaneously during constant stimulation do or do not prevent coherence of oscillatory brain activity between different visual cortical areas. To that goal, we

performed simultaneous recordings in awake macaque areas V1 and V2 and determined within-area gamma peak frequencies and across-area coherence during the presentation of visual stimuli of varying luminance contrast. Furthermore, we tested the extent to which coherence was consistent with a role in neuronal communication by examining the directionality and laminar distribution of gamma-band coherence.

RESULTS

In V1 and V2 Gamma Peak Frequency Is Stimulus Dependent, but Coherence Is Maintained

To test the robustness of gamma coherence across varying stimulus conditions, we simultaneously recorded neuronal activity of V1 and V2 neurons with overlapping or near-overlapping receptive fields (RFs) in two awake macaque monkeys. Spikes and local field potentials (LFPs) were recorded from V1 and V2 using linear arrays of eight recording contacts with a 200 μm intercontact spacing in each area. The monkeys fixated the center of a computer screen while static square-wave gratings of varying luminance contrast were presented in the RFs (Figure S1 available online). In 17 recording sessions from monkey S and 17 from monkey K, we obtained a total of 202 recording sites in V1 and 220 in V2 (monkey S V1 = 107, V2 = 109; monkey K V1 = 95, V2 = 111). To investigate cross-area coherence, we transformed our data into current source density (CSD) by taking the second spatial derivative of the LFP along the linear array electrodes (Mitzdorf, 1985). Using CSD rather than LFP enhances the spatial specificity of coherence measurements and removes the common reference, thereby eliminating major sources of spurious coherence (Mitzdorf, 1985). In total, 780 cross-area coherence measurements were made (monkey S = 408, monkey K = 372). For details, see [Supplemental Experimental Procedures \(Receptive field mapping\)](#).

In a first test of the stimulus dependency of gamma, we computed time-resolved, induced LFP power spectra in areas V1 and V2 for a single session from monkey S for gratings of two different contrasts. Figure 1A (top left) shows a distinct gamma band in V1 with peak power at approximately 40 Hz during 50.3% contrast stimulation. A reduction of grating contrast to 16.3% shifted the gamma band in V1 down to about 30 Hz (Figure 1A, bottom left). Remarkably, exactly the same shift in the gamma frequency was also observed in V2 (center column), as well as in the V1-V2 coherence between CSD channels (right column).

Figure 1B shows the population average induced power spectra for each contrast condition in both monkeys and reveals a large contrast-induced shift of the gamma band in V1 (top row), with frequencies at peak power shifting from \sim 20 Hz for low-contrast stimuli to \sim 45 Hz for high-contrast stimuli. Very similar effects were observed in V2 (Figure 1B, middle row) and in the cross-area coherence (Figure 1B, bottom row). We used a Gaussian fitting approach to determine peaks of V1 and V2 power spectra and cross-area coherence spectra ([Supplemental Experimental Procedures \[Spectral peak determination\]](#); Figure S2). Note that we use the term “peak frequency” as shorthand for the frequency with the highest power/coherence in the gamma range. We found a strong dependence of peak fre-

quency on contrast that was similar for LFP power and for cross-area coherence (Figure 1C). A two-way ANOVA with factors “contrast” and “data type” (V1, V2, or coherence) for each monkey separately confirmed that gamma peak frequency was significantly affected by stimulus contrast [monkey S: $F(7,279) = 128.1$, $p < 0.01$; monkey K: $F(7,269) = 196$, $p < 0.001$] but not data type [monkey S: $F(2,279) = 1.8$, $p = 0.17$; monkey K: $F(2,269) = 5.4$, $p = 0.29$]. Interactions were not significant [monkey S: $F(14,279) = 1.2$, $p = 0.25$; monkey K: $F(14,269) = 1.29$, $p = 0.21$]. Interestingly, we found that in a minority of sessions at the lower two contrasts in monkey S (Figure 1C, left), gamma peak frequency was unexpectedly high, reaching up to 30 Hz during 2.5% contrast stimulation (note the wider SE bars at low contrasts; also see Figures 2 and 3).

Figure 2 further illustrates the close relationships among gamma-band peak frequencies in areas V1 and V2 and cross-area coherence (see squared correlation values in figure). Figure 2 shows for all contrasts and sessions a linear relationship between peak frequency in V1 and in V2 (Figures 2A and 2D), between peak frequency in V1 and V1-V2 coherence (Figures 2B and 2E), and between peak frequency in V2 and V1-V2 coherence (Figures 2C and 2F), with data in each case fit by a regression line with a slope close to 1. These data indicate that V1-V2 coherence was robust against large shifts in the gamma frequency band and argues against the view that coherence can only be efficient in a restricted and fixed band of gamma frequencies. Instead, the data indicate that coherence can sustain long-range communication according to the CTC mechanism across a broad spectrum of stimulus-dependent frequencies.

Laminar Distribution of Gamma Coherence Agrees with Anatomical Feedforward Connectivity

Spike-field coherence spectra and band-limited power spectra show that gamma-band activity is stronger in superficial layers than in deep cortical layers (Buffalo et al., 2011; Maier et al., 2011; Smith et al., 2013; Xing et al., 2012b). We hypothesized that gamma cross-area coherence may also show layer specificity. Specifically, if band-limited coherence is related to neuronal communication, then the coherence may be most prominent between sites known to be strongly connected anatomically. V1 origins of anatomical feedforward connections are situated in layers 2, 3, 4A, and 4B (Callaway, 1998; Lund et al., 1975). V1 layers 2 and 3A (i.e., top two-thirds of layer 3), which receive LGN input indirectly via 4C, provide relatively weak output to V2. However, V1 layer 4B provides a strong magnocellular output directly to V2. In addition, V1 layer 3B, which receives input from sublayers 4C α and 4C β (and also 4A), is also a major source of output to V2 (for reviews see Bastos et al., 2012; Callaway, 1998; Nassi and Callaway, 2009). Thus, the strongest anatomical connection between V1 and V2 is the feedforward projection from superficial V1 layers 3B and 4B, which projects to the full extent of layer 4 in V2 (Douglas and Martin, 2004; Felleman and Van Essen, 1991). Since the stimuli were irrelevant to the task and hence were likely to be ignored, we expected functional connectivity to be dominated by a feedforward flow of information. Therefore, as a minimal hypothesis, we expected the pattern of functional connections, revealed by the strongest coherence measurements, to link relatively shallow

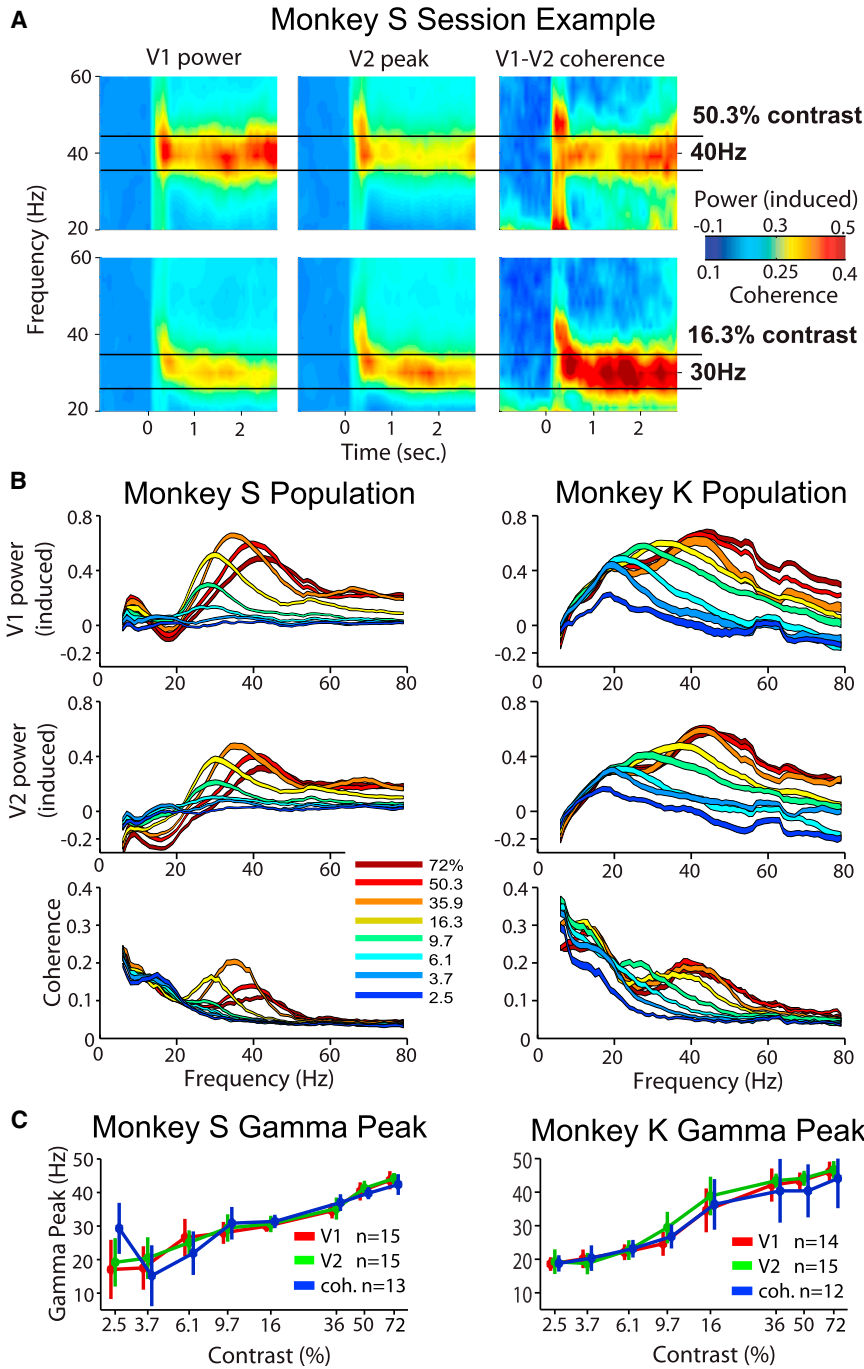


Figure 1. Contrast-Dependent Shift in Gamma Frequency Band

(A) Time-frequency representation of stimulus-induced LFP power in areas V1 (left column) and V2 (middle) and V1-to-V2 coherence (right). Black lines contain the gamma band, which is at a different frequency for different rows (top, 50.3% contrast; bottom, 16.3%).

(B) Stimulus-induced LFP power spectra in V1 (top row) and V2 (middle) and of V1-V2 coherence (bottom) during the sustained period (from 350 ms after stimulus onset) of the response. Line color indicates contrast condition (legend); line thickness indicates SE. Data from two monkeys are shown separately (columns).

(C) Gamma frequency at peak power (derived from data in B; see Figure S2 for details) increases as a function of grating contrast for LFP power in V1 (red line) and V2 (green line) and for V1-V2 coherence (blue line) in monkeys S and K. Error bars show SD.

which, in V1, has been documented to indicate the top of input layer 4C (Maier et al., 2011; Schroeder et al., 1991). The pattern of VEPs across depth in V2 was highly similar to that observed in V1 (note that we were recording on the upper surface of the prelunate gyrus), and we therefore used the same criteria for aligning the V2 data. The point of VEP reversal in V2 was also found to match the point of the early sink-source reversal in the CSD map in that area, which we therefore assume to correspond to the top of layer 4 in V2. In Figure 3, we have set the top of layer 4C as depth zero in V1, and the top of layer 4 in V2 as depth zero in V2. The CSD maps, which were obtained after alignment, and the layer-specific distribution of gamma and of spiking response latencies supported the validity of our alignment procedure (Supplemental Experimental Procedures [Depth alignment procedure and validation]).

After alignment, our minimal hypothesis of a shallower-to-deeper pattern of coherence connections could be reformulated as an expectation of preferential functional connectivity between

sites in V1 with relatively deeper sites in V2. To test this prediction, an alignment of the recording sites from the different depth probe placements over sessions was necessary. This was accomplished by making use of the characteristic reversal in layer 4 from positive visually evoked potentials (VEPs) in superficial layers to negative VEPs in deeper layers (Supplemental Experimental Procedures [Depth alignment procedure and validation]; Figure S3). In the V1 data aligned to the VEP reversal point, we also found a source-sink reversal in the CSD map,

above-zero V1 depths and below-zero V2 depths. As an initial test, we divided all CSD coherence pairs into four groups, with pairs in group 1 linking all V1-V2 sites above zero depth, pairs in group 2 linking all V1-V2 sites below zero depth, pairs in group 3 linking above-zero V1 and below-zero V2 sites, and pairs in group 4 linking below-zero V1 and above-zero V2 sites. A two-way ANOVA, with the factors “group” (four data groupings) and “contrast” (eight contrasts) conducted for each monkey separately, confirmed that gamma

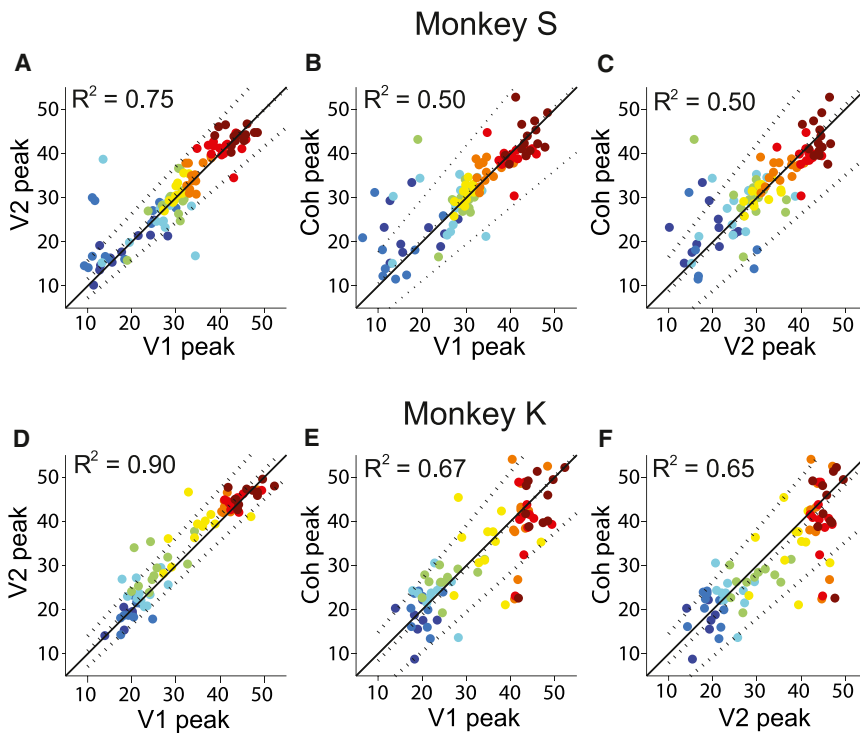


Figure 2. Correlations among Peak Gamma Frequencies

Individual subplots respectively show correlations between the frequency with peak power in V1 LFP (V1 peak) and V2 LFP (V2 peak), the correlation in V1 peak, and the frequency with peak coherence between V1 CSD and V2 CSD (Coh peak) and between V2 peak and Coh peak. Data are shown separately for the two monkeys. Points show peak frequency per session for each contrast condition (dot color codes contrast as in Figure 1B) calculated as the median of the peak frequency recorded at each recording contact or the median the peak frequency of all coherence measurements. Solid black line gives the diagonal. Dashed lines show regression line (largely overlapping with the diagonal) and upper and lower 95% confidence intervals.

coherence significantly depended on data grouping [monkey S: $F(3,3232) = 107.2$, $p < 0.001$; monkey K: $F(3,2800) = 55.9$, $p < 0.001$]. Post hoc testing (Tukey-Kramer method) showed that in both monkeys the above-zero V1 depth to below-zero V2 depth data grouping had significantly higher coherence than other data groupings ($p < 0.05$), in line with the minimal hypothesis outlined above. In agreement with other analyses, the effect of contrast was significant in both monkeys [monkey S: $F(7,3232) = 67.7$; $p < 0.001$, monkey K: $F(7,2800) = 13.4$; $p < 0.001$]. Interactions were significant in monkey S [$F(21,3232) = 3.3$; $p < 0.001$] but not in monkey K [$F(21,2800) = 0.7$, $p = 0.84$].

To investigate the pattern of functional connectivity in the depth-aligned data in a more fine-grained matter, we calculated coherence between all available V1-V2 pairs of CSD contacts. The computation of coherence for V1-V2 pairs of CSD contacts was done for all contrasts in the two monkeys. Grey lines in the 16 panels in Figure 3 indicate all position pairs that were available in our data. Black lines highlight the connections with the strongest coherence (top 5% of the population). In line with the previous analysis, the black lines indicate that the bulk of strong connectivity pairs linked superficial V1 (zero depth and above) with relatively deeper V2 layers (zero depth and below). In monkey S, 63.7% of all strongest coherence pairs linked superficial sites in V1 with deep sites in V2, and in monkey K this was 64.4%.

We then calculated the V1 and V2 center locations of the strong coherence connections as the mean of the depth positions in V1 and V2 of each of the strongest connections. In monkey S, the sites contributing to the strongest connectivity were centered at 0.42 mm in V1 and at -0.24 mm in V2. In

monkey K, this was 0.58 mm in V1 and -0.25 mm in V2 (data combined over contrasts). These values were largely unaffected by stimulus contrast (Supplemental Experimental Procedures [Statistical evaluation of V1-V2 coherence pattern]; Figure S4) and were remarkably similar between monkeys.

We tested the significance of the observed center locations of V1 and V2 against distributions of center locations obtained from a bootstrapping procedure. This procedure confirmed in V2 of both monkeys and in V1 of monkey S that these center locations were significantly different from those expected by chance (this procedure did not yield significant results in V1 of monkey K due to lack of data in deep layers; for details see Figure S4).

We also tested whether the depth range of V1 sites and the depth range of V2 sites forming the pairs of strongest coherence were anatomically plausible. Anatomical studies have shown that the V1 layers most strongly involved in feedforward connectivity comprise layers 4B to 3B, extending about 1 mm above the top of layer 4C; i.e., about 1 mm above the zero-alignment depth in Figure 3 (see also Figure S3). V2 layer 4 is about 0.4 mm thick (de Sousa et al., 2010; Lund, 1988) and should therefore extend below the zero-alignment depth shown in Figure 3 by about 0.4 mm (see also Figure S3). Hence, the strongest anatomical connections originate in a 0–1 mm depth range in V1 and terminate in a 0 to -0.4 mm depth range in V2. These depth ranges capture the large bulk of V1 and V2 depths (79.4% in monkey S and 78.5% in monkey K, pooled over contrasts) contributing to functional connectivity as described in Figure 3. Moreover, the V1 center points (0.42 in monkey S, 0.58 mm in monkey K) fall well within the expected 0 to 1 mm range, and likewise, the V2 center points (-0.24 in monkey S, -0.25 mm in monkey K) fall well within the expected 0 to -0.4 mm range (averaged over contrasts). Hence, we found a remarkable match between the layer-specific pattern of strong functional connectivity (coherence) and the layered pattern of feedforward anatomical connectivity.

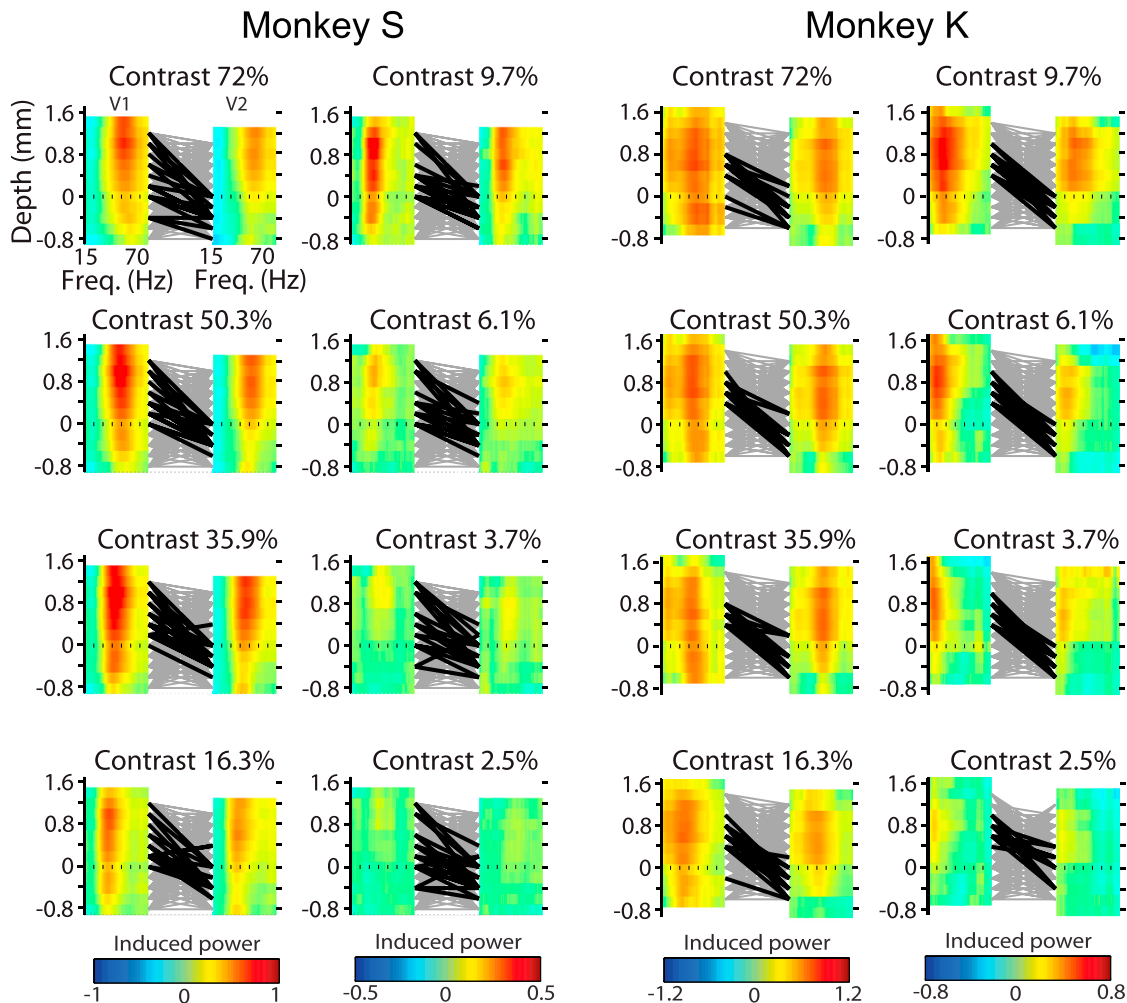


Figure 3. Depth-Specific Pattern of V1-V2 Gamma Coherence Is Preserved across Contrast Conditions

For each of the two monkeys (monkey S on the left and monkey K on the right), there are eight panels. The color surfaces show LFP-induced power as a function of frequency (x axis) and depth (y axis) at each contrast for V1 (leftward) and for V2 (rightward). Horizontal dashed lines in each color surface highlight the 0-depth (top layer 4c in V1 and top layer 4 in V2). Thin gray lines linking V1 and V2 data indicate all pairs of V1/V2 depth positions for which CSD-CSD coherence was recorded. Thick black lines highlight those pairs that showed the strongest coherence (top 5%). Note that there are more depth positions than there are contact points on a single eight-contact probe. This reflects the depth alignment of data coming from different sessions, in which depth probes showed some variability in their physical depth relative to cortex. For details, see Supplemental Experimental Procedures [Depth alignment procedure and validation]; Figure S3.

Directionality Analysis Shows that Gamma Coherence Is Predominantly Feedforward

The coherence-based connectivity displayed in Figure 3 is in line with the known feedforward anatomical connectivity. This suggests that functional directionality analysis for the top 5% strongest coherence pairs in Figure 3 should reveal a predominant feedforward term. To test this idea, we determined Granger causal influences using nonparametric spectral matrix factorization (Dhamala et al., 2008) for the top 5% coherence connections (Figure 4). To quantify the effective directionality, we subtracted the feedback term from the feedforward term. Significance was tested with a bootstrap technique (see Experimental Procedures). We found that the feedforward term (Figures 4A and 4B) was significantly higher than the feedback term (Figures 4C and 4D) at the seven highest contrasts in monkey K (Fig-

ure 4F) and at the three highest contrasts in monkey S (Figure 4E), in line with the previously proposed feedforward function of gamma processes (Buffalo et al., 2011; Bosman et al., 2012). At lower contrasts in monkey S, the feedback term tended to be stronger than the feedforward term, and this difference was significant at the 0.05% level for the 9.7% contrast condition. Note that it was in the same monkey that we observed in a subset of sessions an increase in gamma frequency at the lowest few contrasts compared with higher contrasts (see Figures 1C, 2, and 3). The current Granger analysis suggests that feedback from higher areas could underlie this frequency increase. Granger causal influence spectra showed a shift in peak frequency with stimulus contrast, matching the findings of gamma power and gamma coherence. Hence, despite some differences between monkeys at lower contrasts,

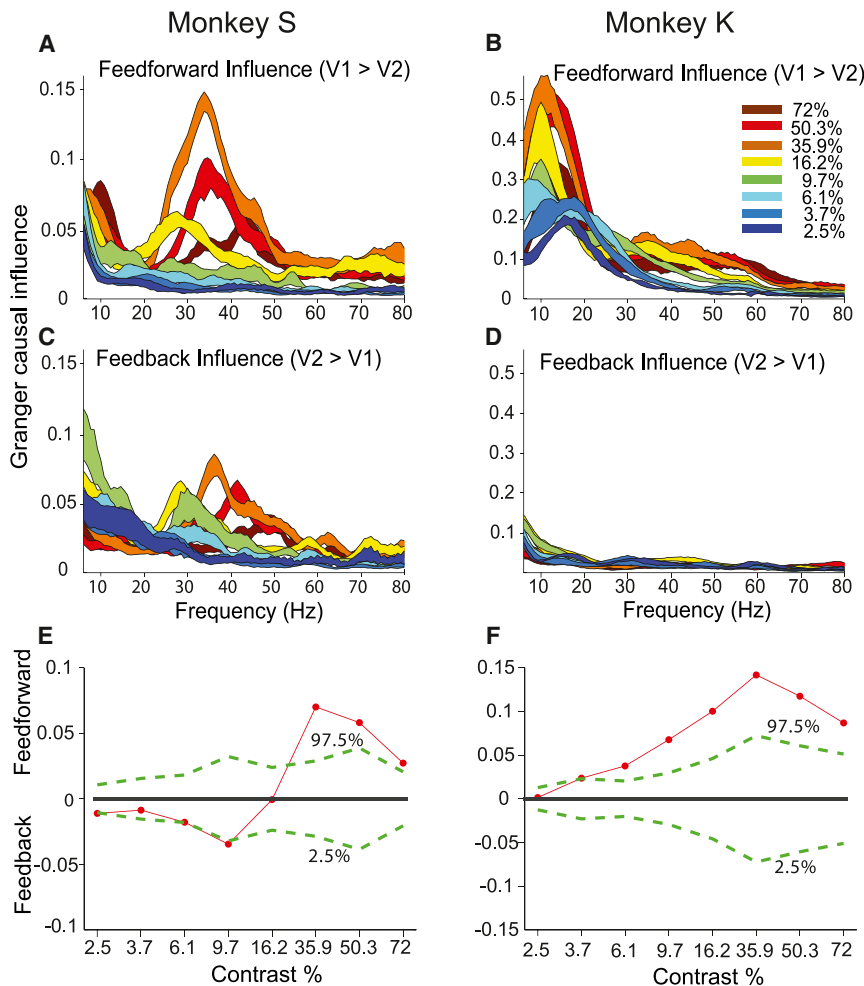


Figure 4. V1-V2 Nonparametric Granger Causality for Different Stimulus Contrasts

Line color indicates contrast condition. Data are shown separately for the two monkeys (columns). (A) and (B) show the feedforward (V1 to V2) term, (C) and (D) show the feedback term (V2 to V1). (E) and (F) show the subtraction of the feedback term from the feedforward term, and the results of the subtractions are shown by red dots and line. Thin green dashed lines show confidence intervals derived from bootstrap testing (described in main text). The significant bias toward feedforward connectivity at higher contrasts in monkey S (contrasts of 35.9% and above) and in monkey K (contrasts of 6.1% and above) remained significant after correction for multiple comparisons (correction for eight tests; resulting in a confidence interval with lower bound 0.31% and upper bound 99.69%).

black lines) showed poor overlap with the reference pattern (shown in red lines), resulting in a low similarity index (yellow color) in the similarity matrix. Test B in monkey S revealed better reference-test similarity, resulting in a higher similarity index (orange color). The similarity was determined between the reference and test patterns for all stimulus contrasts in 25 nonoverlapping 3 Hz frequency windows (i.e., frequency ranges of a 3 Hz width, with their center frequencies increasing from 3 Hz to 78 Hz in steps of 3 Hz; e.g., the first bin containing frequencies from 2 Hz to 4 Hz). In both

monkeys, the highest similarity values were confined to the gamma range (which was broader in monkey K than in monkey S; see Figure 1). The difference between similarity values for all coherence patterns within 10 Hz of the peak gamma frequency and values obtained outside that frequency range was highly significant for both monkeys [two-sample t test: monkey S: $t(174) = 11.9, p < 0.001$; monkey K: $t(155) = 6.5, p < 0.001$]. These findings show that the preservation of layer-specific patterns of V1-V2 functional connectivity is specific to the gamma range. This further supports gamma as a means of stable neural communication despite large stimulus-induced gamma frequency changes. In addition, the tight link between the stable V1-V2 coherence connections and gamma gives further support to the notion that these connections are predominantly feedforward, as in other studies gamma has indeed been linked with feedforward information transmission (Buffalo et al., 2011).

The Similarity of V1-V2 Gamma Coherence Networks Is Maintained over Contrast

Granger causality analysis support a feedforward flow of information in both monkeys at higher contrasts.

The coherence networks presented in Figure 3 appear highly similar for different contrast conditions. In Figure 5, we tested this similarity, and moreover we tested whether the layer-specific similarity of functional connections for different contrasts was limited to the gamma band. To quantify similarity, we first defined the pattern observed at the maximum power (peak) gamma frequency at a midlevel contrast of 35.9% as a “reference pattern” of layer-specific coherence. In Figure 5, the reference is labeled “R” in the similarity matrices of monkeys S and K. We compared this reference to “test patterns” observed with the other contrasts, with four example test patterns labeled A–D in the similarity matrices. To do the comparison in a robust way, we rank-ordered the coherence values and subsequently calculated a measure of similarity as the percentage of variance in the test pattern explained by the reference pattern. The small panels in Figure 5 show visual illustrations of comparison tests between the reference pattern (red lines) and test patterns (black lines). For example, for test A in monkey S, test pattern A (shown in

monkeys, the highest similarity values were confined to the gamma range (which was broader in monkey K than in monkey S; see Figure 1). The difference between similarity values for all coherence patterns within 10 Hz of the peak gamma frequency and values obtained outside that frequency range was highly significant for both monkeys [two-sample t test: monkey S: $t(174) = 11.9, p < 0.001$; monkey K: $t(155) = 6.5, p < 0.001$]. These findings show that the preservation of layer-specific patterns of V1-V2 functional connectivity is specific to the gamma range. This further supports gamma as a means of stable neural communication despite large stimulus-induced gamma frequency changes. In addition, the tight link between the stable V1-V2 coherence connections and gamma gives further support to the notion that these connections are predominantly feedforward, as in other studies gamma has indeed been linked with feedforward information transmission (Buffalo et al., 2011).

Rapid Shifts in Gamma Band Frequency under Constant Stimulus Conditions

Rapid, apparently random shifts in frequency as observed in striate cortex (Burns et al., 2011; Xing et al., 2012a) could present an important barrier for effective communication though coherence, in addition to stimulus-dependent shifts. These shifts

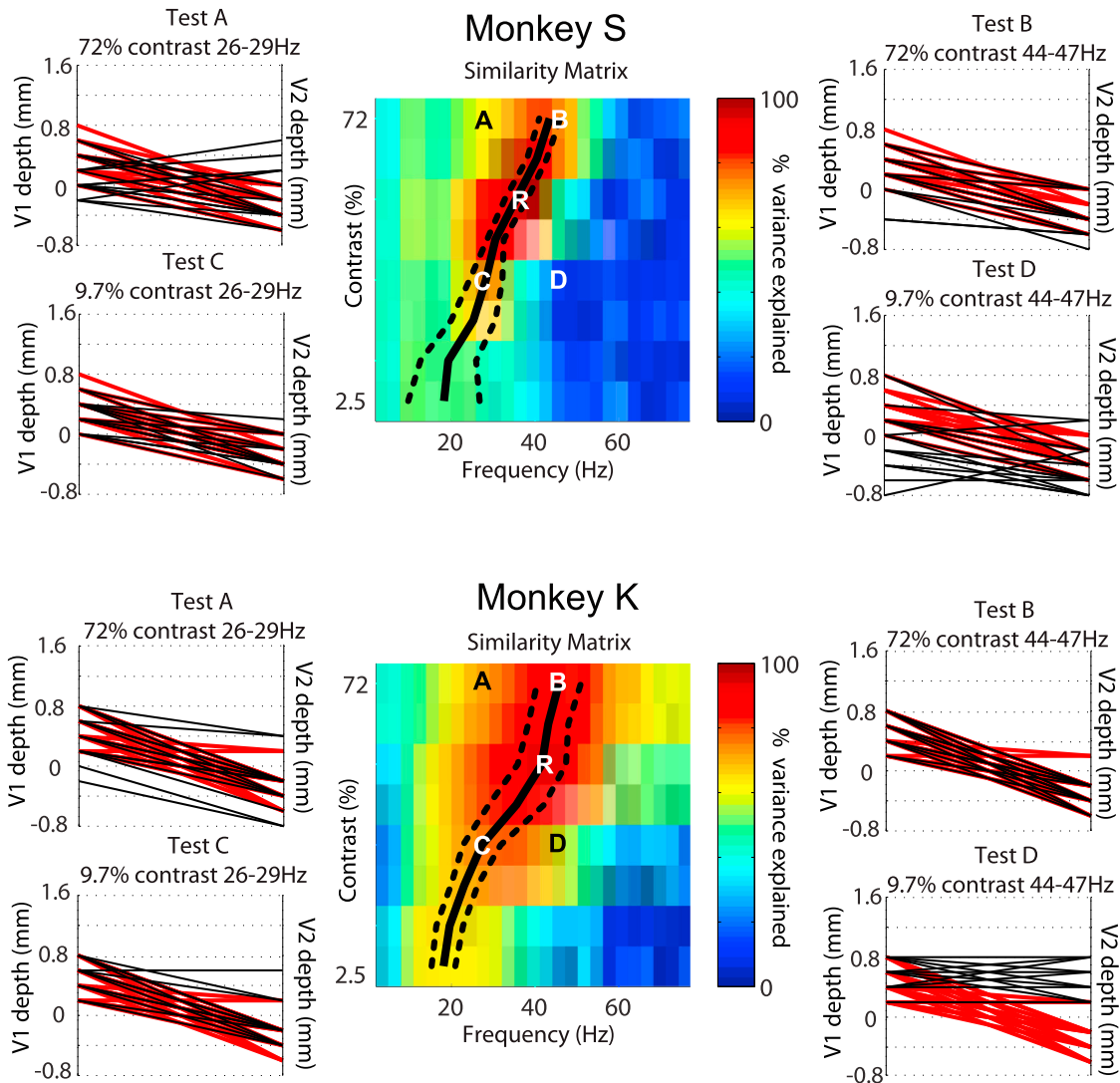


Figure 5. Quantitative Comparison of the Cross-Area Coherence Pattern across Frequencies and Contrast Conditions in Monkeys S and K Surface color shows the similarity (percentage variance explained) between the test coherence patterns for each contrast at each 3 Hz frequency window and the reference pattern (marked by an R on the color surface). For each contrast, V1-V2 coherence was computed in each 1 Hz bin (Hanning tapered), and bins were grouped in 3 Hz windows within which coherence values were averaged. Similarity values were computed by comparing reference to test patterns of connectivity at a frequency resolution of 3 Hz. For each contrast, reference-test similarity was shown for 25 nonoverlapping 3 Hz frequency windows (with center frequencies from 3 to 78 Hz increasing with a step size of 3). Thus, for example, the first window was centered on 3 Hz containing frequencies from 2 to 4 Hz, the second window was centered on 6 Hz containing 5–7 Hz, etc. The overlaid black line in the color surfaces for each monkey shows mean peak gamma frequency per contrast condition (mean calculated from data from V1 and V2 combined, and flanking dashed lines indicate ± 1 SD; data are shown separately in Figure 1C). This line closely tracks the peak similarity in the color surfaces. Surrounding plots (test A–D) show examples comparisons of connectivity patterns for selected test patterns (A–D as marked in color surfaces) and the reference pattern R. Red lines show the top 5% coherence pairs in the reference pattern, and black lines show the top 5% coherence pairs for the test patterns. Each comparison of reference and test patterns yields a similarity index shown on a color scale in the color surface representing the similarity matrix. Letters marking test and reference patterns are colored black or white for visibility.

could represent physiological fluctuations in stimulus drive as well as noise within cortical networks. Since we observed robust coherence between V1 and V2, this suggests the existence of a mechanism that limits frequency differences between V1 and V2 on brief time scales. To test whether our data support such mechanism, we characterized moment-by-moment variation in gamma peak frequency in V1 and V2. Following Burns et al. (2011), one might expect higher areas (V2) to be unlikely to

keep up with changing frequency in lower areas (V1). Figure 6A shows V1 frequency versus V2 frequency joint probability scatter diagrams for three contrasts from a single session of monkey S, with marginal distributions of the probability of frequency in V1 and V2 along x and y axes, respectively. Figure 6B shows population data from the two monkeys for four contrasts using joint probability surfaces. Figures 6A and B show that the frequency estimates within V1 and V2 varied over up to 15 Hz, confirming

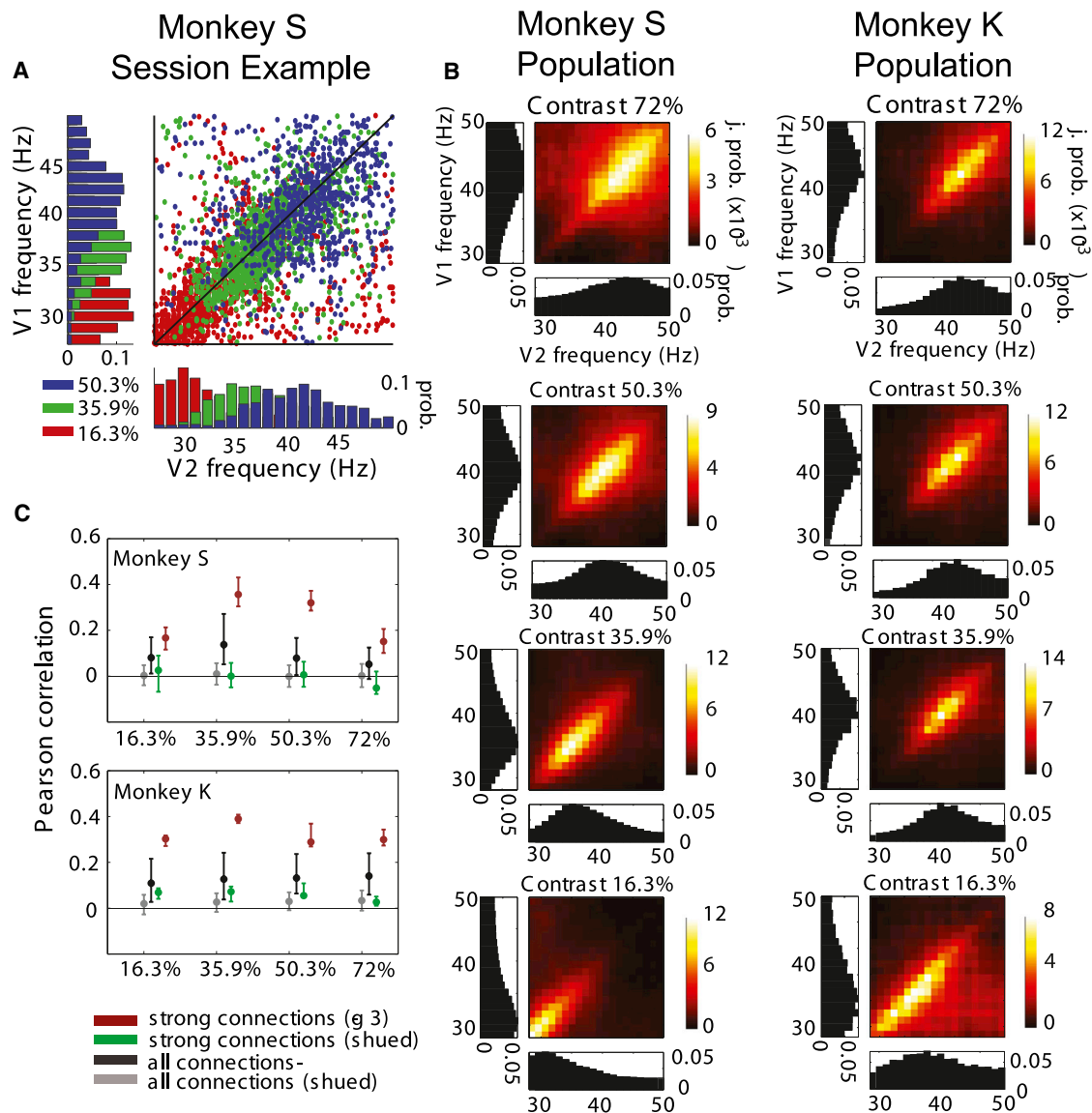


Figure 6. Evidence for Frequency-Frequency Matching

(A) Moment-by-moment frequency-frequency correlation from a single V1-V2 pair of sites from a single example session in monkey S at three stimulus contrasts. Each dot represents the frequency of the ongoing LFP of V1 (y ordinate) and V2 (x ordinate) at a specific 1 ms time bin. The black line gives the diagonal. Histograms along the axes show the probability distribution per frequency.

(B) Population joint probability (j. prob.) of V1/V2 frequency-frequency coupling for four contrasts (row titles) for monkey S (left) and monkey K (right). Histograms along the axes show the probability distribution per frequency.

(C) Median of frequency-frequency correlation coefficients for different contrasts in the population of V1-V2 connections. Correlations are shown without shuffling based on all connections (black symbols) or based on the top 5% strongest coherence connections (red symbols). In addition, correlations are shown after trial shuffling, again for all connections (gray symbols) and for the 5% strongest connections (green symbols). Error bars show upper and lower quartiles.

Burns et al's findings in V1 (Burns et al., 2011). Given this large frequency range in each area, a high correlation is not expected unless there is a mechanism that helps to constrain frequency differences between the two areas. In our data, we find a strong probability for frequency-frequency matches (bottom-left to top-right diagonal in joint probability surfaces) and a significant moment-to-moment frequency-frequency correlation. Pearson V1-V2 correlations in moment-to-moment gamma frequency

are illustrated in Figure 6C for four contrasts. These correlations were in the order of 0.1 when based on all possible V1-V2 contact pairs, pooled over both monkeys and all sessions (dark gray symbols in Figure 6C). For the 5% strongest connections shown in Figure 3, correlation coefficients were in the order of 0.3 pooled over monkeys and contrasts (red symbols in Figure 6C). To test the significance of the correlations, we randomly shuffled trial labels between V1 and V2 and recalculated

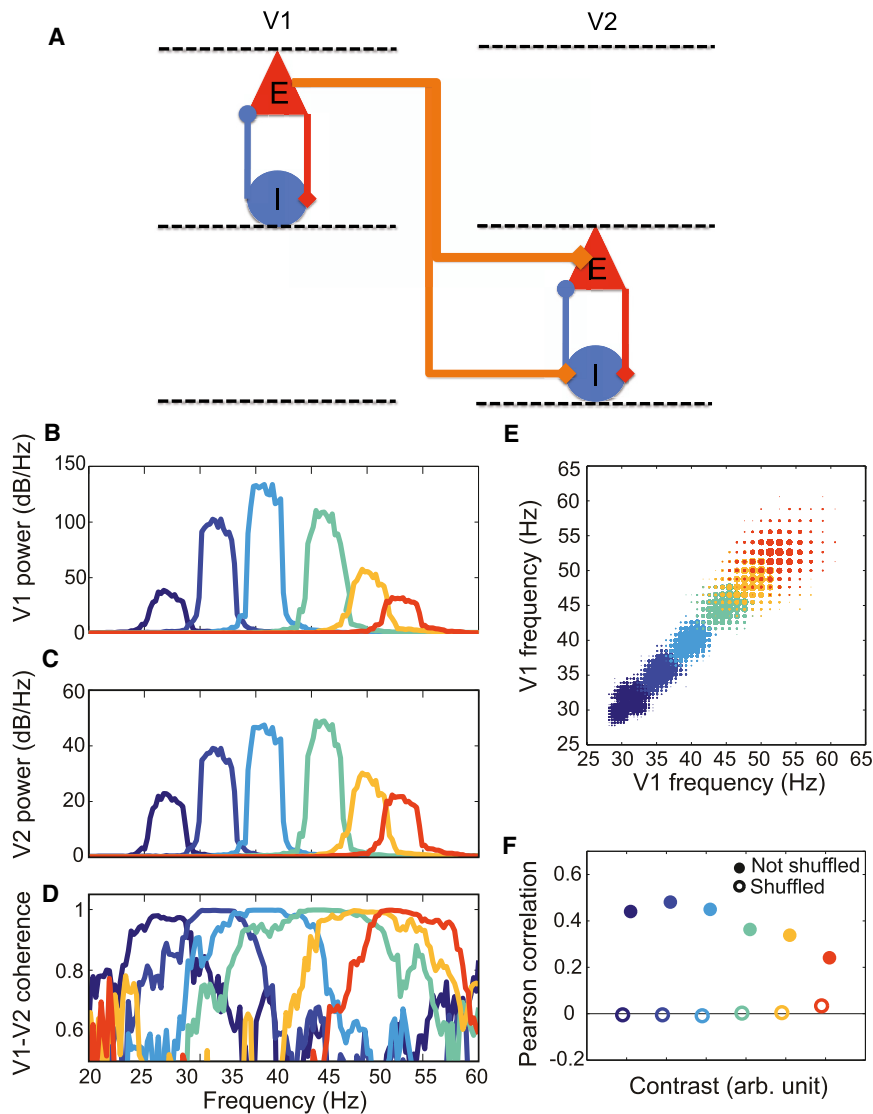


Figure 7. Simulation of Frequency-Frequency Matching between V1 and V2

(A) Schematic representation of reciprocally coupled network of excitatory (E, red) and inhibitory cells (I, blue) within V1 and V2. In each area, the network contained 400 E cells and 100 I cells. Forward projection was modeled by E cells in superficial V1 projecting to both E as well as I cells in layer 4 of V2 (orange lines); the projections between areas were stronger than within-area projections of the same type. E-to-E projections were a factor 4 stronger and E-to-I projections were 5/3 times stronger (Supplemental Experimental Procedures [Computational model]; Table S2). The visual stimulation was modeled by a constant depolarizing current to the E and I cells in V1, together with a slowly fluctuating, zero-mean drive. Stochastic fluctuations represented stimulus-induced stochastic fluctuations in the layer 4 activity, which provides the input to V1 superficial layer. Stimulus contrast was modeled as the level of depolarization, and the time-varying firing rate of the E cells was taken as a proxy for the LFP. Additional model description and parameter settings are presented in the Supplemental Experimental Procedures (Computational model).

(B–F) Frequency analysis of simulated oscillations in V1 and V2 for different contrast values, varying from the lowest contrast in blue to the highest contrast in red. The gamma band shifted to higher frequencies with increased “contrast” in V1 (B) and V2 (C), which is also reflected in the near-unity value for coherence between V1 and V2 at those common peak frequencies (D). The power at the peak frequency varied nonmonotonously with a maximum at intermediate frequencies, which reflects an optimal frequency for within-area synchronization set by the synaptic time scale of fast inhibition. The analysis in (B)–(D) was based on average power over a long time range (3 s). Despite modeled fluctuations in driving current, there was frequency matching between V1 and V2 on a short time scale (E; dot size represents number of observations, ranging between 1 and 352 per dot). This led to significant correlations in the time-resolved peak frequencies (for all contrasts $p < 0.0001$), which were lost when V2 time series were shuffled (F).

correlation coefficients over 1,000 iterations. The distribution of correlation coefficients was not significantly different from 0 in shuffled data, and correlation coefficients in the unshuffled data were significantly above the shuffled distribution (all $p < 0.005$ for both monkeys). These data support the idea of a functional architecture that helps constrain frequency-frequency differences on short time scales during communication (coherence) between two recorded cortical areas. The high correlation of rapid frequency shifts in the two cortical areas could reflect rapid shifts in the internal state of the animal (Gray and McCormick, 1996) that simultaneously and equally affects both cortical areas. However, Granger causality analysis (Figure 5) indicates a predominantly feedforward influence of V1 onto V2, especially at high stimulus contrasts, so it is also possible that the gamma peak frequency in V2 is dynamically matched to the incoming V1 gamma signal.

Dynamic Frequency Matching Is Obtained in Coupled PING Models

To elucidate the mechanism by which gamma frequency in a downstream area dynamically shifts in order to match the frequency of an upstream area, we have constructed a computational model in which local V1 and V2 networks were modeled explicitly by spiking neurons with Hodgkin-Huxley voltage-gated channels. The V1 network consisted of reciprocally connected excitatory (E) and inhibitory (I) neurons. V2 was modeled in the same way, with the E and I cells in addition receiving direct excitatory inputs from V1 E cells. We have illustrated these networks as respectively representing superficial V1 and layer 4 of V2 (Figure 7A). Within each network, all cells received noise currents (details in Supplemental Experimental Procedures [Computational model]). Each network synchronized through the pyramidal interneuron gamma (PING) mechanism, in which a volley of

E cells recruits a volley of I cells. This shuts the network down for a gamma period, and when the E cells recover, the cycle starts anew. For the oscillations to be present, the E cells need to be depolarized (for example, by presentation of a stimulus), and the frequency of oscillations then depends on the level of depolarization in the E and I cells. The level of depolarizing current in the model was set at six levels, simulating a variation in contrast (Sanchez-Vives et al., 2000) from low to high (dark blue to red colors in Figures 7B–7F). This accounts for the stimulus-induced oscillations in V1 at different simulated contrasts (Figure 7B). Stimulus-induced oscillations in V2 can arise by the same mechanism, but in the simulation the stimulus-related inputs to V2 come from V1, and therefore are already oscillating at gamma. Hence, the V2 network activity locks to the oscillating input, which is indicated by power peaks in corresponding frequencies in V1 and V2 (Figures 7B and 7C) and coherence between V1 and V2 in the same frequency band (Figure 7D). Simulated contrast increases led to enhanced power reaching a maximum at intermediate frequencies, with diminishing power for further simulated contrast increases (Figures 7B and 7C). During the time interval that the simulated stimulus was present, the V1 gamma frequency fluctuated in a 5–10 Hz frequency band, reflecting simulated variations in driving current (noise; details in Supplemental Experimental Procedures [Computational model]). Despite these rapid frequency fluctuations, there were significant correlations of moment-to-moment peak frequencies in V1 and V2 (Figure 7E), indicating a form of dynamic frequency matching between V1 and V2. Correlation coefficients for different contrasts ranged between 0.24 and 0.48 and all were significant (based on the same approach and criteria as used for empirical data). The correlations were nonsignificant when the peak-frequency time series was shuffled (Figure 7F). There were, however, limitations to the frequency range within which, and the rate of frequency change for which, frequency matching between PING networks could be obtained. For example, when V1 frequency changed by more than 20 Hz in 200 ms, V2 frequencies no longer matched V1 frequencies. Taken together, our modeling study shows that two PING networks, in which one provides forward drive to the other, produce an output that closely resembles our empirical observations (compare Figures 7B–7D with Figures 1B and 7E to 6A). Hence, the frequency of gamma oscillations in different populations exchanging information may not only be determined by local architecture in each area, but appears to be influenced by interactions among those populations. The interconnection of PING networks thus provides a mechanism that may be highly relevant for our empirical observations. This mechanism may underlie the entrainment or mutual interactions between communicating neural populations that are necessary to offset initial differences in oscillation frequencies to thereby initiate and maintain communication between distant neural populations.

DISCUSSION

We have shown that CTC between V1 and V2 remains possible despite significant stimulus and time-dependent changes in gamma frequency, because these changes occur in a coordinated fashion between areas. Other authors have proposed

that coherence (synchrony) may be an important mechanism for “binding” the representation of single stimuli among neurons within the same area—the so-called binding by synchrony hypothesis (Gray et al., 1989). This hypothesis is conceptually distinct from the CTC hypothesis, which emphasizes the contribution of coherence to long-range, interareal communication. Note, however, that there is also some overlap between the two hypotheses, as coherent activity from distributed neurons at a lower stage of the cortical hierarchy may be more effectively integrated by later-stage neurons, indicating that binding also implies coherent interareal communication. Therefore, critical ideas on the relevance of synchrony/coherence for binding have immediate implications for CTC, and vice versa. Hence, although our data only addressed CTC directly, we here discuss our findings in the context of both theories.

Binding by Synchrony

The theoretical proposal of binding by synchrony has attracted both support (Gray, 1999; Singer and Gray, 1995) and criticism (Palanca and DeAngelis, 2005; Thiele and Stoner, 2003). Of particular relevance for the idea of binding through within-area synchronous activity to distributed object parts, Ray and Maunsell (2010) showed that pairs of V1 neurons responding to different parts of a single contrast-varying grating (Gabor stimulus) responded with differing peak gamma frequencies, in line with our own data. Moreover, they showed reduced gamma coherence compared to conditions where contrast did not vary over the object surface, suggesting that binding by synchrony may not operate effectively for parts within an object characterized by different contrast and different gamma frequency. Hence, the Ray and Maunsell’s study and ours both point to the importance of a sufficient frequency match between different neuronal populations for maximizing neuronal communication by synchrony or coherence. From their interesting data, Ray and Maunsell (2010) concluded that binding by synchrony may be problematic for contrast-varying objects in V1. This prediction, however, should be followed up by further experiments before we can fully exclude a synchrony-based mechanism for binding. For example, Ray and Maunsell (2010) did not assess the monkey’s perceptual experience of the object. It is possible that for large-contrast differences, bright parts of the stimulus are seen as the foreground and darker as the background, or vice versa (Manjunath and Chellappa, 1993). Furthermore, we have recently shown attentional modulation of gamma frequency (Bosman et al., 2012), and we therefore speculate that attentional mechanisms could potentially reduce gamma frequency differences between neurons representing an attended object, which may be especially relevant in stimuli, or stimulus parts, showing smaller variations in contrast. Hence, we suggest that not only in CTC but also in binding, the presence or absence of frequency differences is perceptually relevant and may, within constraints, be exploited by executive mechanisms (such as attention).

Communication through Coherence

The peak-power frequency of gamma oscillations has been shown to vary considerably between individuals but has been thought to be largely stable within individuals (Hoogenboom

et al., 2006; Muthukumaraswamy et al., 2010). A stable frequency might be considered to be an attractive attribute for theories that propose neuronal synchrony to underlie long-range communication (Fries, 2005; Salinas and Sejnowski, 2001; Tiesinga et al., 2002; Wildie and Shanahan, 2012), as stability would help to ensure that distant cortical areas maintain matching oscillation frequencies. Under conditions of nonstable frequency, an additional assumption must be made; namely, that frequency shifts in separate areas occur in unison.

Until recently, only minor shifts in peak frequency with changes in stimulus characteristics (Gray et al., 1990; Swettenham et al., 2009) and state of the animal (Feng et al., 2010) were demonstrated. These effects were generally relatively small (on the order of 5 Hz or less, but see Gieselmann and Thiele, 2008) and were not widely considered to represent a major challenge to the assumption of a stable intraindividual gamma band. However, we found a much stronger stimulus dependency of gamma frequency, varying from 18 Hz at the lowest contrast (2.8%) to 45 Hz at the highest (78%), in line with Ray and Maunsell (2010). Interestingly, recordings in anesthetized macaque reported no change in frequency with varied contrast (Henrie and Shapley, 2005), which may be due to anesthesia: Xing et al. (2012a) demonstrated a substantial reduction in gamma frequency during anesthesia that may limit the dynamic range for further modulation of frequency by stimulus contrast. Large stimulus-dependent shifts in frequency agree with computational network models (Buia and Tiesinga, 2006; Traub et al., 1996; but see also Vida et al., 2006) as well as in vitro (Linás et al., 1991; Traub et al., 1996) and in vivo experiments (Atallah and Scanziani, 2009) linking oscillation frequency with excitatory drive (see also Figure 7), which in those studies may be equated with stimulus contrast (Sanchez-Vives et al., 2000).

As local architecture of visual areas may lead to differences in their stimulus dependency of gamma (Buzsáki and Chrobak, 1995), gamma power may be contained in different frequency bands for the same stimulus in different areas. As a sufficient frequency match of oscillatory activity is important to achieve phase coupling and coherence, CTC (Fries, 2005) can be expected to be limited if gamma frequencies in different areas are too disparate. In the latter case, the relationship between excitable periods in different populations of neurons would vary over time, thereby limiting neuronal communication. This limitation in principle could be circumvented without any need for an active frequency-matching mechanism if the gamma band were sufficiently broad, shifted only slightly with stimulus variations, and maintained sufficient overlap in V1 and V2 for any stimulus condition. In that case, neural communication between areas could be maintained through coherence between common frequencies in the power spectra for each area, even if the power at these overlapping frequencies would be limited. However, our data demonstrate that the impact of stimulus contrast on V1 gamma frequency is powerful enough that, were V2 gamma frequency unaffected by contrast, changes in local gamma due to stimulus contrast could potentially move the frequency band of gamma synchrony in V1 so far away from the frequency band of gamma synchrony in V2 that gamma as a channel for communication would become unlikely. Furthermore, gamma frequency was found to be unstable in both areas,

varying over a range of ~ 15 Hz from moment to moment. Were this variation to occur independently, gamma frequencies in the two areas would be incompatible for a large part of the time, even if time-averaged peak frequencies matched; thus, rapid and non-stimulus-dependent shifts in frequency would present an additional obstacle to effective communication.

However, we found that (1) the power spectra of the LFP in V1 and V2 showed similar shifts in peak power as a function of stimulus contrast, (2) the same peak shift occurred in the coherence between V1 and V2, (3) the pattern of coherence between V1 and V2 was layer specific and matched the pattern expected according to feedforward anatomical connectivity, (4) the pattern was robust against large variations in stimulus contrast, and (5) rapid and non-stimulus-dependent shifts in gamma frequency were highly correlated in V1 and V2, consistent with a frequency-matching mechanism that was modeled successfully by a computational neuronal network comprising two interconnected PING networks. Thus, cross-area coherence was maintained in an anatomically consistent pattern over conditions of widely and rapidly varying gamma frequency, in line with a role of coherence in neural communication. The evidence emerging in this research field that neural communication through coherence does not require a fixed gamma frequency, and that gamma frequency differences can make or break communication links, suggests that frequency differences could be exploited as a mechanism to route information in the brain during perceptual and cognitive operations.

EXPERIMENTAL PROCEDURES

Species Used and Surgical Procedures

Two male *Macaca mulatta* were used in this study. All procedures were in accordance with the European Communities Council Directive 1986 (86/609/EEC) and approved by the local ethics committee (Radboud University Dier Experimenten Commissie). Following initial training, monkeys were implanted with a titanium head holder (Crist Instrument) and a recording chamber (NaN instruments) above V1/V2 under general anesthesia and sterile conditions. In a second surgery, after further training, a craniotomy was made above V1/V2.

Stimuli

Stimuli were presented on a Samsung TFT screen (SyncMaster 940bf, $38^\circ \times 30^\circ$ 60 Hz). Stimuli were circular patches (typical diameter of 5° , but varied in some sessions between 1° and 9°) of static (not drifting) square-wave gratings (two cycles/degree), at luminance contrasts of 2.5%, 3.7%, 6.1%, 9.7%, 16.3%, 35.9%, 50.3%, or 72%. Stimuli were presented at two orthogonal orientations. Average luminance matched the background (125 cd/m^2). Stimulus presentation time was randomized between 750 and 4,000 ms and was preceded by 1,000 ms prestimulus time. During stimulation and prestimulus time, the monkey maintained an eye position (measured by an infrared camera, Arrington 60 Hz sampling rate) within a square window of $2 \times 2^\circ$. This window was relatively large to allow for noise associated with the camera. Eye position was considerably more stable than the window allowed. The median difference in eye position from one trial to the next was 0.23° in monkey S and 0.5° in monkey K. This excludes the possibility that the large grating stimuli centered on the RFs of the recorded neurons would have left the RFs on any of the trials. The median total range in eye position within trials, as measured with the Arrington system, was 0.8° in monkey S and 0.45° in monkey K. These values likely underestimate the true accuracy of fixation. In later experiments in monkey S, we have used a high-speed infrared camera system (Thomas Recording 245 Hz system) in conjunction with the Arrington system. Using the Thomas recording system, we recorded a more stable eye position, with a within-trial median total range in eye position of 0.3° . Since RFs were small

relative to the size and spatial frequency of the grating, eye movements in the order of a few tenths of a degree would be too small to radically change the nature of the stimulation.

Recording Methods

Spikes and LFP were recorded using two linear arrays of eight recording contacts (Plexon) with 200 μm intercontact spacing. Recording arrays were manipulated using NaN instruments microdrives. LFPs were filtered (0.7–300 Hz) and recorded at 1 KHz (Plexon MAP system). The probes were placed 4 to 6 mm apart such that RFs from the two areas were overlapping or near-overlapping (mean overlap of simultaneously recorded V1 and V2 RF areas = 14.3%; SD = 22.3%). Regions with close RFs are likely to have stronger anatomical connections (Lund et al., 2003), and stronger coherence (Bosman et al., 2012; Nowak et al., 1999), than regions with distant RFs. In our data, cross area CSD coherence was not found to be correlated with V1-V2 RF distance in monkey S ($R^2 = 0.0002$, $p = 0.5$ robust linear regression) and was only weakly (negatively) correlated in monkey K ($R^2 = 0.003$, $p = 0.039$). This indicates that the daily variation in the amount of RF overlap was insufficient to affect coherence.

Data are included from 17 recording sessions from monkey S and 17 from monkey K. In total, data are included from 202 recording sites in V1 and 220 in V2 (monkey S: V1 = 107, V2 = 109; monkey K: V1 = 95, V2 = 111). Deeper sites that we could document, based on receptive field mapping, to not belong to the area of interest were excluded from these counts (see Supplemental Experimental Procedures [Receptive field mapping]). We collected an average of 62 trials per condition per session in monkey S and 53 trials per condition per session in monkey K. In analyses of responses in single areas (V1 or V2 separately), all available data were used. In analysis of V1-V2 coherence, functional connectivity, and frequency-frequency correlation, less data could be included because data were missing in either V1 or V2 of some sessions (for example, because of a probe not sufficiently entering cortex). Coherence and functional connectivity analyses in monkey S were based on 13 sessions with data from both areas (2 sessions were rejected because of missing V1 data, and 2 sessions were rejected because of missing V2 data). In monkey K, these analyses were based on 12 sessions with data from both areas (3 sessions were rejected because of missing V1 data, and 2 sessions were rejected because of missing V2 data).

RFs were mapped using high-contrast black and white squares presented individually at a fast rate, on a 10×10 grid, with square sizes varying from 0.1° to 1° . Averaged over monkeys (who showed similar values), RF sizes were 0.75° in V1 (5.4° eccentricity) and 0.91° in V2 (5.9° eccentricity). V2 recordings were done on the prelunate gyrus. Data were classified as belonging to V1 or V2 based on conventional criteria (Gattass et al., 1981; see Supplemental Experimental Procedures [Definition of the V1/V2 border]).

Data Selection

The first 500 ms following fixation onset and the first 350 ms following stimulus onset were discarded from data analysis to avoid effects of fixation-onset and stimulus-onset transients. In addition to the large shift (~ 25 Hz) of peak gamma frequency with increases in grating contrast, we also observed much smaller shifts (~ 1 – 2 Hz) as a function of stimulus size and orientation. In the analyses presented in the main text, data were pooled across all size and orientation conditions per contrast.

Power and Coherence Computations

Stimulus-induced power (psi) in the LFP signal was computed from nonoverlapping 500 ms (or 1,000 ms for analysis shown in Figure 5) time windows starting 350 ms after stimulus onset (S). LFP spectra were computed using a multitaper method with discrete prolate spheroid sequences for frequencies of 6 to 80 Hz (smoothing ± 3 Hz), or for analysis of 1,000 ms snippets (Figure 4), using Hanning tapers for frequencies between 2 and 80 Hz and 2 Hz frequency resolution (Oostenveld et al., 2011). Power generally decreases as a function of frequency (f) in a $1/f$ manner. Hence, power in higher-frequency bands can be difficult to discern, and power spectra recorded in the stimulation period (S) was indexed against power spectra recorded during the prestimulus baseline (B) computed over the 500 ms prior to stimulus onset [$\text{Psi} = (S - B)/(S + B)$]. The $1/\text{frequency}$ drop-off of power spectra was thus removed from the data. Coherence was calculated as the magnitude of the summed cross-spectral

density between two CSD time series, normalized by respective power spectra (Oostenveld et al., 2011).

Granger Calculation

We used a nonparametric spectral matrix factorization of the CSD cross-spectral density (calculated from the period of 350 ms after stimulus onset, to the trial end) to estimate feedforward and feedback influences for a given V1-V2 contact pair (Dhamala et al., 2008) using the Fieldtrip toolbox (Oostenveld et al., 2011). To test for significance for an unidirectional dominance in Granger influence over different contrasts, the difference between feedforward and feedback terms was recomputed 10,000 times with randomized feedback and feedforward labels of V1-V2 pairs to estimate the null distribution of the effective directionality. For significance testing, the frequency range of 20–55 Hz was used. At each randomization iteration, we subtracted the maximum value of the feedback term from the maximum value of the feedforward term. Correspondingly, a unidirectional dominance was considered to be significant if it reached the top or bottom 2.5 percentile of the null distribution. In Figure 5, data were pooled over all V1-V2 contact pairs with 5% strongest coherence values.

Frequency-Frequency Locking Estimation

To assess the moment-to-moment evolution of oscillation frequency in the gamma range, we estimated the frequency based on complex Morlet wavelet time-frequency CSD representations for each trial (wavelet width $\sigma = 5$ ms). For a given 1 ms time bin, the peak power in the frequency range 25–55 Hz was recorded and only peak power that differed by $>2\sigma$ from baseline power was included. Four different contrasts (16.3%, 35.9%, 50.3%, and 72%) were included. At lower contrasts, gamma oscillations were partly intermixed with other processes operating at alpha/beta frequency regime. In Figure 6A, an example of a V1-V2 contact pair (from monkey S) is shown with frequency-frequency scatterplot and marginal distribution for three different contrasts (16%, 35.9%, and 50.3%). Figure 6B shows combined joint probability surfaces and marginal distributions from all contact pairs in the population. To quantify the strength of the correlation, we then computed the Pearson correlation for each contact pair. To test for significance, a randomization procedure was implemented by shuffling trial labels. Significance testing was done as for Granger estimates. In Figure 6C, the median and interquartile range of the distribution is shown for randomized and nonrandomized overall distribution as well as the distribution of 5% strongest coherence connections highlighted in Figure 3. We found significant correlation coefficients (that is, outside of 97.5% of the shuffled data distribution) over the population and especially for the strongest coherence connections.

SUPPLEMENTAL INFORMATION

Supplemental Information includes four figures and Supplemental Experimental Procedures and can be found with this article online at <http://dx.doi.org/10.1016/j.neuron.2013.03.003>.

ACKNOWLEDGMENTS

This research was supported by NWO VICI grant 453-04-002 (to P.D.W.), NWO VENI grant 451-09-025 (to M.R.), and Maastricht University graduate funding in cooperation with the Donders Institute for Brain Behavior and Cognition (to P.D.W.). Experiments were designed by P.D.W. and M.R. Measurements were carried out by M.R. and E.L. with assistance from N.B. Analysis was carried out by M.R. and E.L. and modeling by M.T.W. with guidance from P.T., P.F., and P.D.W. The paper was written by M.R., E.L., and P.D.W. in collaboration with the other authors.

Accepted: February 28, 2013

Published: May 8, 2013

REFERENCES

Atallah, B.V., and Scanziani, M. (2009). Instantaneous modulation of gamma oscillation frequency by balancing excitation with inhibition. *Neuron* 62, 566–577.

- Bastos, A.M., Usrey, W.M., Adams, R.A., Mangun, G.R., Fries, P., and Friston, K.J. (2012). Canonical microcircuits for predictive coding. *Neuron* 76, 695–711.
- Bosman, C.A., Schoffelen, J.M., Brunet, N., Oostenveld, R., Bastos, A.M., Womelsdorf, T., Rubehn, B., Stieglitz, T., De Weerd, P., and Fries, P. (2012). Attentional stimulus selection through selective synchronization between monkey visual areas. *Neuron* 75, 875–888.
- Buffalo, E.A., Fries, P., Landman, R., Buschman, T.J., and Desimone, R. (2011). Laminar differences in gamma and alpha coherence in the ventral stream. *Proc. Natl. Acad. Sci. USA* 108, 11262–11267.
- Buia, C., and Tiesinga, P. (2006). Attentional modulation of firing rate and synchrony in a model cortical network. *J. Comput. Neurosci.* 20, 247–264.
- Burns, S.P., Xing, D., and Shapley, R.M. (2011). Is gamma-band activity in the local field potential of V1 cortex a “clock” or filtered noise? *J. Neurosci.* 31, 9658–9664.
- Buzsáki, G., and Chrobak, J.J. (1995). Temporal structure in spatially organized neuronal ensembles: a role for interneuronal networks. *Curr. Opin. Neurobiol.* 5, 504–510.
- Buzsáki, G., and Draguhn, A. (2004). Neuronal oscillations in cortical networks. *Science* 304, 1926–1929.
- Callaway, E.M. (1998). Local circuits in primary visual cortex of the macaque monkey. *Annu. Rev. Neurosci.* 21, 47–74.
- de Sousa, A.A., Sherwood, C.C., Schleicher, A., Amunts, K., MacLeod, C.E., Hof, P.R., and Zilles, K. (2010). Comparative cytoarchitectural analyses of striate and extrastriate areas in hominoids. *Cereb. Cortex* 20, 966–981.
- Dhamala, M., Rangarajan, G., and Ding, M. (2008). Analyzing information flow in brain networks with nonparametric Granger causality. *Neuroimage* 41, 354–362.
- Douglas, R.J., and Martin, K.A. (2004). Neuronal circuits of the neocortex. *Annu. Rev. Neurosci.* 27, 419–451.
- Felleman, D.J., and Van Essen, D.C. (1991). Distributed hierarchical processing in the primate cerebral cortex. *Cereb. Cortex* 1, 1–47.
- Feng, W., Havenith, M.N., Wang, P., Singer, W., and Nikolić, D. (2010). Frequencies of gamma/beta oscillations are stably tuned to stimulus properties. *Neuroreport* 21, 680–684.
- Fries, P. (2005). A mechanism for cognitive dynamics: neuronal communication through neuronal coherence. *Trends Cogn. Sci.* 9, 474–480.
- Gattass, R., Gross, C.G., and Sandell, J.H. (1981). Visual topography of V2 in the macaque. *J. Comp. Neurol.* 201, 519–539.
- Gieselmann, M.A., and Thiele, A. (2008). Comparison of spatial integration and surround suppression characteristics in spiking activity and the local field potential in macaque V1. *Eur. J. Neurosci.* 28, 447–459.
- Gray, C.M. (1999). The temporal correlation hypothesis of visual feature integration: still alive and well. *Neuron* 24, 31–47, 111–125.
- Gray, C.M., and McCormick, D.A. (1996). Chattering cells: superficial pyramidal neurons contributing to the generation of synchronous oscillations in the visual cortex. *Science* 274, 109–113.
- Gray, C.M., König, P., Engel, A.K., and Singer, W. (1989). Oscillatory responses in cat visual cortex exhibit inter-columnar synchronization which reflects global stimulus properties. *Nature* 338, 334–337.
- Gray, C.M., Engel, A.K., König, P., and Singer, W. (1990). Stimulus-Dependent Neuronal Oscillations in Cat Visual Cortex: Receptive Field Properties and Feature Dependence. *Eur. J. Neurosci.* 2, 607–619.
- Henrie, J.A., and Shapley, R. (2005). LFP power spectra in V1 cortex: the graded effect of stimulus contrast. *J. Neurophysiol.* 94, 479–490.
- Hoogenboom, N., Schoffelen, J.M., Oostenveld, R., Parkes, L.M., and Fries, P. (2006). Localizing human visual gamma-band activity in frequency, time and space. *Neuroimage* 29, 764–773.
- Jia, X., Xing, D., and Kohn, A. (2013). No consistent relationship between gamma power and peak frequency in macaque primary visual cortex. *J. Neurosci.* 33, 17–25.
- Llinás, R.R., Grace, A.A., and Yarom, Y. (1991). In vitro neurons in mammalian cortical layer 4 exhibit intrinsic oscillatory activity in the 10- to 50-Hz frequency range. *Proc. Natl. Acad. Sci. USA* 88, 897–901.
- Lund, J.S. (1988). Anatomical organization of macaque monkey striate visual cortex. *Annu. Rev. Neurosci.* 11, 253–288.
- Lund, J.S., Lund, R.D., Hendrickson, A.E., Bunt, A.H., and Fuchs, A.F. (1975). The origin of efferent pathways from the primary visual cortex, area 17, of the macaque monkey as shown by retrograde transport of horseradish peroxidase. *J. Comp. Neurol.* 164, 287–303.
- Lund, J.S., Angelucci, A., and Bressloff, P.C. (2003). Anatomical substrates for functional columns in macaque monkey primary visual cortex. *Cereb. Cortex* 13, 15–24.
- Maier, A., Aura, C.J., and Leopold, D.A. (2011). Infragranular sources of sustained local field potential responses in macaque primary visual cortex. *J. Neurosci.* 31, 1971–1980.
- Manjunath, B.S., and Chellappa, R. (1993). A unified approach to boundary perception: edges, textures, and illusory contours. *IEEE Trans. Neural Netw.* 4, 96–108.
- Mitzdorf, U. (1985). Current source-density method and application in cat cerebral cortex: investigation of evoked potentials and EEG phenomena. *Physiol. Rev.* 65, 37–100.
- Muthukumaraswamy, S.D., Singh, K.D., Swettenham, J.B., and Jones, D.K. (2010). Visual gamma oscillations and evoked responses: variability, repeatability and structural MRI correlates. *Neuroimage* 49, 3349–3357.
- Nassi, J.J., and Callaway, E.M. (2009). Parallel processing strategies of the primate visual system. *Nat. Rev. Neurosci.* 10, 360–372.
- Nowak, L.G., Munk, M.H., James, A.C., Girard, P., and Bullier, J. (1999). Cross-correlation study of the temporal interactions between areas V1 and V2 of the macaque monkey. *J. Neurophysiol.* 81, 1057–1074.
- Oostenveld, R., Fries, P., Maris, E., and Schoffelen, J.M. (2011). FieldTrip: Open source software for advanced analysis of MEG, EEG, and invasive electrophysiological data. *Comput. Intell. Neurosci.* 2011, 156869.
- Palanca, B.J., and DeAngelis, G.C. (2005). Does neuronal synchrony underlie visual feature grouping? *Neuron* 46, 333–346.
- Ray, S., and Maunsell, J.H. (2010). Differences in gamma frequencies across visual cortex restrict their possible use in computation. *Neuron* 67, 885–896.
- Ray, S., and Maunsell, J.H. (2011). Different origins of gamma rhythm and high-gamma activity in macaque visual cortex. *PLoS Biol.* 9, e1000610.
- Rosenblum, M., Pikovsky, A., and Kurths, J. (2001). Synchronization: A Universal Concept in Nonlinear Sciences (Cambridge Nonlinear Science Series) (Cambridge, UK: Cambridge University Press).
- Salinas, E., and Sejnowski, T.J. (2001). Correlated neuronal activity and the flow of neural information. *Nat. Rev. Neurosci.* 2, 539–550.
- Sanchez-Vives, M.V., Nowak, L.G., and McCormick, D.A. (2000). Membrane mechanisms underlying contrast adaptation in cat area 17 in vivo. *J. Neurosci.* 20, 4267–4285.
- Schroeder, C.E., Tenke, C.E., Givre, S.J., Arezzo, J.C., and Vaughan, H.G., Jr. (1991). Striate cortical contribution to the surface-recorded pattern-reversal VEP in the alert monkey. *Vision Res.* 31, 1143–1157.
- Singer, W., and Gray, C.M. (1995). Visual feature integration and the temporal correlation hypothesis. *Annu. Rev. Neurosci.* 18, 555–586.
- Smith, M.A., Jia, X., Zandvakili, A., and Kohn, A. (2013). Laminar dependence of neuronal correlations in visual cortex. *J. Neurophysiol.* 109, 940–947.
- Swettenham, J.B., Muthukumaraswamy, S.D., and Singh, K.D. (2009). Spectral properties of induced and evoked gamma oscillations in human early visual cortex to moving and stationary stimuli. *J. Neurophysiol.* 102, 1241–1253.
- Thiele, A., and Stoner, G. (2003). Neuronal synchrony does not correlate with motion coherence in cortical area MT. *Nature* 421, 366–370.

- Tiesinga, P.H., Fellous, J.M., José, J.V., and Sejnowski, T.J. (2002). Information transfer in entrained cortical neurons. *Network* 13, 41–66.
- Traub, R.D., Whittington, M.A., Colling, S.B., Buzsáki, G., and Jefferys, J.G. (1996). Analysis of gamma rhythms in the rat hippocampus in vitro and in vivo. *J. Physiol.* 493, 471–484.
- Vida, I., Bartos, M., and Jonas, P. (2006). Shunting inhibition improves robustness of gamma oscillations in hippocampal interneuron networks by homogenizing firing rates. *Neuron* 49, 107–117.
- Wildie, M., and Shanahan, M. (2012). Establishing communication between neuronal populations through competitive entrainment. *Front. Comput. Neurosci.* 5, 1–16.
- Xing, D., Shen, Y., Burns, S., Yeh, C.I., Shapley, R., and Li, W. (2012a). Stochastic generation of gamma-band activity in primary visual cortex of awake and anesthetized monkeys. *J. Neurosci.* 32, 13873–80a.
- Xing, D., Yeh, C.I., Burns, S., and Shapley, R.M. (2012b). Laminar analysis of visually evoked activity in the primary visual cortex. *Proc. Natl. Acad. Sci. USA* 109, 13871–13876.